





Full Length Article

Structural and optical properties of iron ions doped near-infrared persistent spinel-type phosphors

L. Pan^{a, c}, Y. Wang^a  , L. Yin^a, M. Zhang^a, Y. Li^a, P.D. Townsend^b, D. Poelman^c

^a School of Science, China University of Geosciences, Beijing, 100083, China

^b Physics Building, University of Sussex, Brighton, BN1 9QH, UK

^c LumiLab, Dept. Solid State Sciences, Ghent University, Ghent, Belgium

Received 22 December 2022, Revised 19 March 2023, Accepted 21 March 2023, Available online 24 March 2023, Version of Record 28 March 2023.

<https://doi.org/10.1016/j.jlumin.2023.119822>

Structural and optical properties of iron ions doped near-infrared persistent spinel-type phosphors

L Pan^{1,3}, Y Wang^{1*}, L Yin¹, M. Zhang¹, Y. Li¹, P. D. Townsend², D. Poelman³

¹School of Science, China University of Geosciences, Beijing, 100083, China

²Physics Building, University of Sussex, Brighton, BN1 9QH, UK

³LumiLab, Dept. Solid State Sciences, Ghent University, Ghent, Belgium

* Corresponding author: wxfemail@gmail.com

Abstract: In this work, a series of iron ions doped spinel-type compounds AB_2O_4 were prepared by high temperature solid phase reactions. The phase compositions all the samples were analyzed using X-ray diffraction (XRD). Thermoluminescence (TL), and persistent luminescence spectra were collected systematically to reveal the trapping and de-trapping processes. Photoluminescence (PL) bands in the near-infrared luminescence band (600 to 900 nm) were observed for all the Fe^{3+} -doped spinel-type structured materials. It was demonstrated that $MgGa_2O_4:Fe^{3+}$ sample showed the best persistent luminescence (PersL) performance among the compounds studied. X-ray Photo Electron Spectroscopy (XPS) and Electron Paramagnetic Resonance Spectroscopy (EPR) tests reveal that the dopant Fe ions have a greater probability of occupying the octahedral sites than tetrahedral sites. Thanks to its long persistence, $MgGa_2O_4:Fe^{3+}$ has the potential to be used in the biological or agricultural related applications.

Keywords: Fe ions; spinel structure; persistent luminescence; $MgGa_2O_4:Fe^{3+}$

1. Introduction

Persistent phosphors are a type of light-storing luminescent materials that slowly emit energy in the form of light after excitation (e.g. high-energy rays, visible light, ultraviolet light, etc.). The light can be emitted continuously for minutes to hours after the excitation stops. Phosphors with persistent luminescence have been rapidly developed in the past decades. Among them, near-infrared (NIR) PersL materials are extremely attractive in biomarker imaging, anti-counterfeiting, information encryption, and optical

information storage [1-5].

The most commonly used luminescent ions for NIR long persistent luminescent materials are based on Cr^{3+} emitters [6]. However, chromium ion-doped luminescent materials are a questionable choice for bioimaging related application because Cr^{6+} is toxic and may raise bio-safety concerns although the amount of doping is very limited [7-10]. Therefore, the development of chromium-free NIR emitters is very urgent. As an essential element for the human body, the non-toxic and inexpensive Fe^{3+} is one of the suitable candidate dopant ions to solve these problems. Fe^{3+} has a similar electronic configuration as the Mn^{2+} ion and has been found to show near-infrared photoluminescence in diverse hosts, with emission peaks in the red or near-infrared (${}^4\text{T}_1({}^4\text{G}) \rightarrow {}^6\text{A}_1({}^6\text{S})$ transition) [11-13]. However, research on Fe^{3+} -doped PersL materials is very limited since Fe^{3+} ions are usually used as quenchers rather than luminescence centers. Recently, $\text{SrAl}_{12}\text{O}_{19}:\text{Fe}^{3+}$ was prepared by using a synthetic method of chemical precipitation and its afterglow period has been greatly extended [14]. Fe^{3+} activated LiGaO_2 phosphor with high fluorescence intensity and near-infrared afterglow performance has been reported [15]. A new strategy for defect-enriched activated Fe^{3+} ion luminescence was proposed [16]. Even though, there are still very few studies and reports on Fe^{3+} -doped afterglow luminescent materials and the relevant afterglow mechanism is not yet clear. So it is important to explore special crystal structures and modulate the defect properties in suitable matrices to explore Fe^{3+} -doped NIR PersL phosphors.

It is widely known that crystal structure and local structure are closely related to optical properties of materials. Since the spinel structure is very prone to the formation of vacancies, gaps and anti-site defects, it is one of the best crystal structures for designing PersL materials [17, 18]. Spinel, with structural formula AB_2O_4 , are ionic compounds, generally with an Fd-3m space group belonging to the cubic crystal system as shown in Figure 1a. A in the structural formula represents a divalent metal ion (cation) occupying a tetrahedral position inside a face-centered cubic lattice, while B represents a trivalent metal ion (cation)

occupying an octahedral position in a face-centered cubic crystal structure. Under certain conditions, the crystal structure tends to form a mixed spinel structure (Figure 1b), where the A- and B-site atoms are randomly assigned to occupy the tetrahedral and octahedral sites. For example, it is reported that under high temperature solid phase sintering, ZnGa_2O_4 exhibits an inversion rate of about 3%, which means that the octahedral position is occupied by 3% of the Zn^{2+} ions [19]. The mutual substitution between the A and B site cations leads to inherent defects (anti-site defects), which can act as trapping centers for the charge carriers generated through the radiation, while the different symmetries of coordination environments and the different strengths of the crystal fields would have an effect on the luminescence properties of Fe^{3+} .

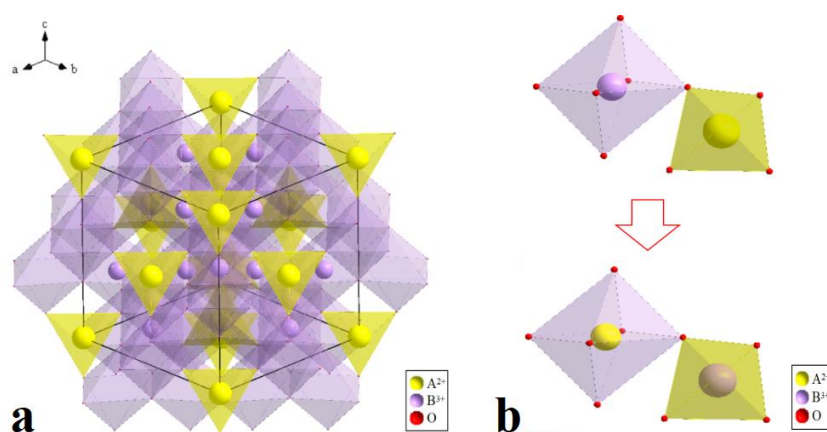


Figure 1a. Diagram of spinel structure. b. Illustration of possible anti-site defects in the material.

In this work, a series of pure AB_2O_4 ($\text{A}=\text{Zn}, \text{Mg}, \text{B}=\text{Ga}, \text{Al}$) and Fe^{3+} doped AB_2O_4 spinel-type structured materials have been prepared. Luminescence properties, especially PersL related characteristics are comprehensively surveyed. In order to study the tendency of Fe^{3+} ions to occupy different crystalline positions, Electron Paramagnetic Resonance Spectroscopy (EPR) and X-ray Photo-electron Spectroscopy (XPS) data have been obtained.

2. Experimental

All samples (pure AB_2O_4 and 5mol% Fe^{3+} doped AB_2O_4) in this work were synthesized via a high

temperature solid-state route. According to the stoichiometric ratio, raw materials, ZnO (99.99%, Kwangfu Fine Chemical Industry Research Institute), MgO (99.95%, Alfa Aesar), Ga₂O₃ (99.99%, Kwangfu Fine Chemical Industry Research Institute), Al₂O₃ (99.99%, Alfa Aesar) and Fe₂O₃ (Kwangfu Fine Chemical Industry Research Institute) were mixed respectively and placed into alumina crucibles according to the stoichiometric ratio. ZnGa₂O₄ (ZGO), ZnGa₂O₄: Fe³⁺ (ZGO: Fe³⁺), ZnAl₂O₄ (ZAO) and ZnAl₂O₄: Fe³⁺ (ZAO: Fe³⁺) samples were sintered at 1450 °C for 6 h while MgGaO₄ (MGO), MgGaO₄: Fe³⁺ (MGO: Fe³⁺), MgAl₂O₄ (MAO) and MgAl₂O₄: Fe³⁺ (MAO: Fe³⁺) were prepared at 1300 °C for 6 hours. For easy comparison, the doping concentration was kept fixed at 5mol% for all the samples. The samples were then ground into fine powders after being naturally cooled down to room temperature.

X-ray diffraction (XRD) patterns of as-prepared samples were collected by using an XD-1 diffractometer with Cu K α ($\lambda=1.5406$ Å) as a radiation source. The scanning speed was 8 °/min with the 2 θ scanning range from 10 ° to 90 °.

PL excitation and emission spectra and persistent luminescence excitation (PersLE) spectra were collected using a FluoroMax-4 (Horiba) spectrometer equipped with a Xenon lamp.

X-ray photoelectron spectroscopy (XPS) and the valence state of Fe was analyzed by using a ESCALAB 250Xi (Thermo Fisher (USA)) spectrometer with monochromatized Al α X-ray beam (1486.6 eV). The binding energies were calibrated by fixing the C1s peak at 284.6 eV.

The Electron paramagnetic resonance (EPR) spectra were recorded at room temperature using a Bruker A300 (Germany) spectrometer operating at X-band frequency (~ 9.2 GHz) and a field modulation at 100 kHz.

Thermoluminescence (TL) measurements of the samples were recorded with a TOSL-3DS spectrometer made by the Guangzhou Ruidi Aisheng Technology Co. Ltd. The linear heating rate was 3 °C/s

and the temperature range was from 30 °C to 450 °C .

3. Results and discussion

3.1. XRD

The powder XRD patterns of as-prepared and 5mol% Fe doped spinel-type compounds AB_2O_4 (A = Zn, Mg and B = Ga, Al) are shown in **Figure 2**. The major diffraction peaks of the materials are consistent with the standard powder diffraction cards. All the recorded diffraction peaks from samples are well matched to those in the standard card which confirms that the prepared samples are in pure phase and the doping of Fe ions does not cause the obvious changes to the crystal structure of the host.

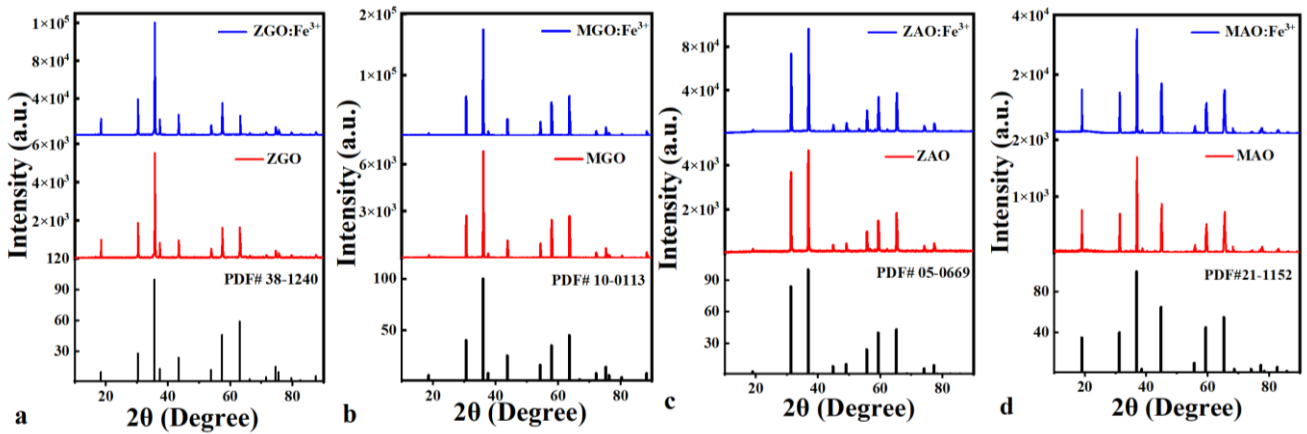


Figure 2. XRD patterns of samples with pure and Fe^{3+} -doped spinel-type compounds. (PDF#38-1240, PDF#05-0669, PDF#21-1152 and PDF#10-0113 are the standard cards of $ZnGa_2O_4$, $ZnAl_2O_4$, $MgAl_2O_4$ and $MgGa_2O_4$ in JADE respectively).

3.2. Photoluminescence properties

PL emission spectra of samples $ZGO: Fe^{3+}$, $MGO: Fe^{3+}$, $ZAO: Fe^{3+}$ and $MAO: Fe^{3+}$ are shown in the right hand part of **Figure 3**. Upon excitation at 254 nm, all samples exhibit a broad emission band from the red to near infrared range, with peaks at 702 nm, 687 nm, 703 nm and 744 nm, corresponding to the spin-forbidden ${}^4T_1 ({}^4G) \rightarrow {}^6A_1 ({}^6S)$ electronic transition of trivalent iron ions [20]. The shift of the peak wavelength for these four samples indicated that the luminescence sites of Fe^{3+} are strongly influenced by the crystal field environments even they have the same spinel typed crystal structure. The excitation spectra

of the samples are collected by monitoring the peak emission of Fe^{3+} which are presented in the left part of **Figure 3**. The main broad absorption bands in the 240-325 nm range are ascribed to the $\text{O}^{2-} \rightarrow \text{Fe}^{3+}$ charge transfer band [21-23] which differs between samples. Besides, the other weaker excitation bands from left to right are attributed to the ${}^6\text{A}_1 ({}^6\text{S}) \rightarrow {}^4\text{E} ({}^4\text{D})$, ${}^4\text{T}_2 ({}^4\text{D})$ and ${}^4\text{T}_2 ({}^4\text{G})$ d-d transitions, respectively [24].

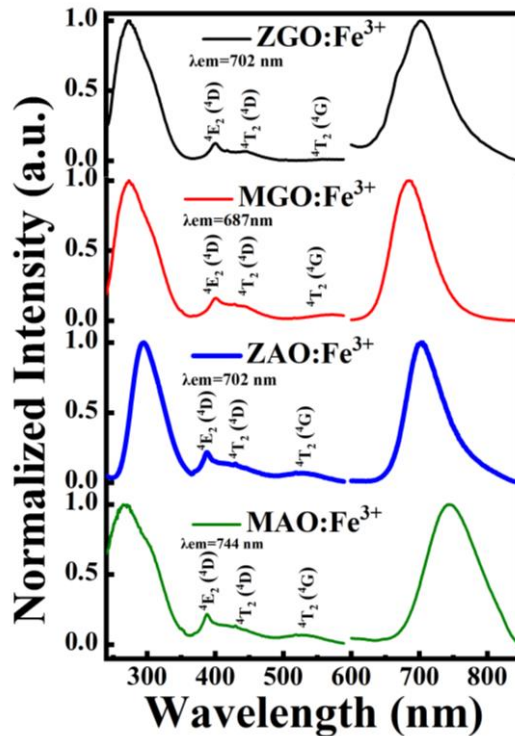


Figure 3. Normalized PL excitation spectra of Fe^{3+} -doped spinel-type structured materials by monitoring the Fe^{3+} emission at peak wavelength (left) and the emission spectra under UV excitation at 254 nm (right).

3.3. Persistent luminescence

After being irradiated with a 254 nm mercury lamp for 5 minutes, the persistent luminescence decay curves of all the iron doped samples were monitored at the peak wavelength of PersL spectra which are the same with PL spectra but with lower intensities. The obtained decay curves are shown in **Figure 4a**. Among these samples, MGO: Fe^{3+} exhibits the strongest afterglow and longest persistent time, followed by the sample of ZGO: Fe^{3+} . Since Cr^{3+} -doped samples of spinel structures that have been extensively studied, especially ZGO:Cr^{3+} , it is worthwhile to compare the persistent decay curves of two types of samples to give one an idea on the performance of these Fe^{3+} -doped samples. Thus, long period persistent decay curves were

recorded for both sample MGO: Fe³⁺ and ZGO:Cr³⁺, as shown in Figure 4b. The result indicates that the intensity is still higher than the background signal even after 16 hours, suggesting that both materials have good persistent luminescence properties. It is a pity that the performance of MGO:Fe³⁺ is not yet as good as ZGO:Cr³⁺, although the Fe³⁺ doped persistent material has had less development. In order to obtain effective NIR PersL excitation bands of MGO: Fe³⁺ sample, different excitation wavelengths were used to irradiate the sample. The excitation wavelength ranged from 630 nm to 200 nm with a step of 10 nm. Then the persistent luminescence excitation spectra of MGO: Fe³⁺ were obtained by plotting the beginning afterglow intensity with the irradiation wavelength, as shown in Figure 4c. PLE spectra was added for comparison. It can be noticed that the PersEL is much narrower than PLE, but the optimum excitation wavelength for NIR PersL is around 260 nm which matches well with the excitation wavelength of PL. Therefore, the effective capture of charge carriers of PersL should be assisted by host absorption and/or Fe-O band excitation [25-27]. Besides, there is an additional small peak around 550 nm which is corresponding to the transition from the ground state energy level ⁶A₁ (⁶S) to the excited state energy level ⁴T₂ (⁴G) of Fe³⁺ ions. Although it is relatively weak, it implies that PersL signals of this material can be obtained under low-energy light with multiple times of excitation which means this new PersL luminescent material may have great advantage as vivo bioimaging probe.

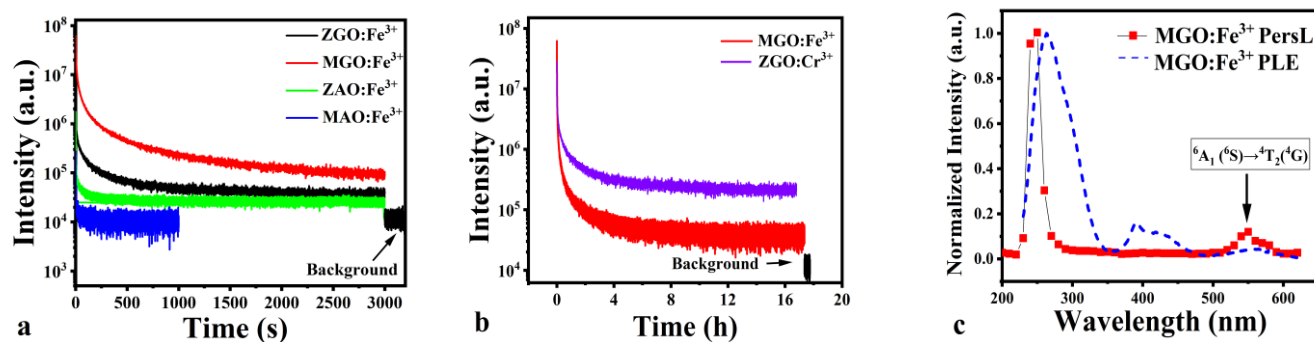


Figure 4a. The persistent luminescence decay curves of Fe ion-doped spinel structure materials after excitation by a 254 nm ultraviolet lamp for 5 minutes b. PersL decay curve (recorded for more than 16 h) of MGO: Fe³⁺ and the ZnGa₂O₄: 5 mol% Cr³⁺ sample after illumination for 5 min with 254 nm UV lamp. c. PersL excitation spectra (PersLE) of MGO: Fe³⁺ (recorded at 20 s after stopping the excitation).

3.4 Thermoluminescence spectra

The TL technique is a common method to obtain trap-related information, including the depth and distribution of traps as well as the charge carrier motion. etc. TL curves of the Fe^{3+} doped compounds monitored at different emission wavelengths after removal of the 254 nm excitation for 5 min are shown in **Figure 5**. 3D plots of the samples are shown in the left, and the corresponding contour maps are in the right. TL results of three samples which include ZGO: Fe^{3+} , MGO: Fe^{3+} and ZAO: Fe^{3+} exhibit strong NIR emission spectra of Fe^{3+} . However, there is no thermoluminescence signal for MAO: Fe^{3+} . There is an additional emission band around 510 nm which appears only in the TL results from ZGO: Fe^{3+} and MGO: Fe^{3+} samples. Since these two samples are gallium acid based materials, the cause of the emission must be gallium related which is assigned to the electronic transition of Ga^{3+} ions (octahedrally coordinated) to O^{2-} [28]. It is noticed that TL of MGO: Fe^{3+} is the most intense among these samples, followed by the sample of ZGO: Fe^{3+} . TL results are well matched with the persistence performance of samples and indicate that MGO and ZGO are promising matrices for Fe^{3+} doped persistent phosphor materials although MGO: Fe^{3+} has better performance with the doping concentration of 5mol%.

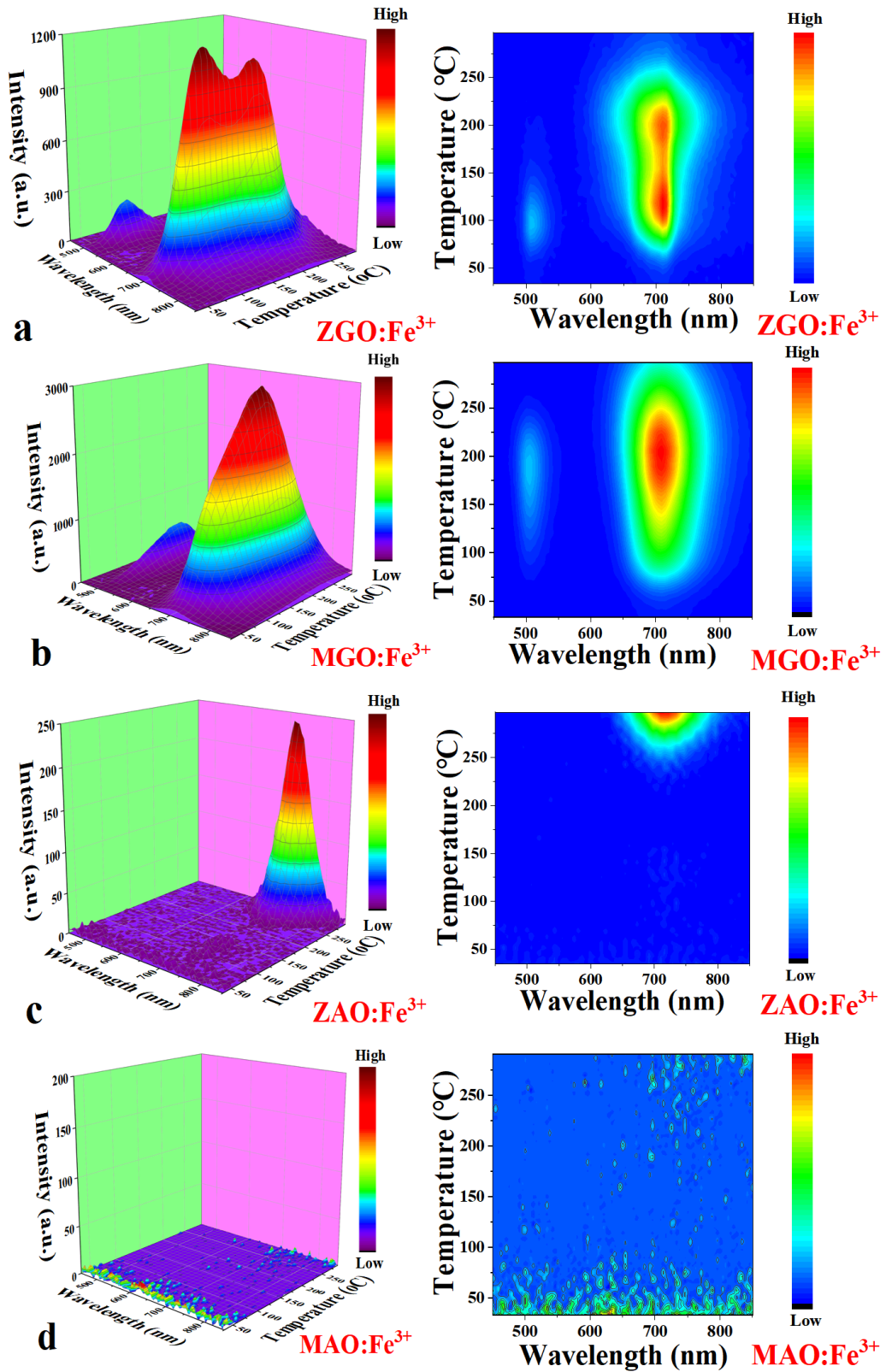


Figure 5. 3D plots of TL of ZGO:Fe³⁺, MGO:Fe³⁺, ZAO:Fe³⁺ and MAO:Fe³⁺ samples after excitation by 254 nm UV light for 5mins. The corresponding contour maps are shown on the right.

TL glow curves of Fe doped spinel-type samples have been integrated from 650-800 nm range according to the data in Figure 5, as shown in Figure 6a. The normalized glow curves are shown in Figure

6b for easy comparison. It has been noted that TL results can reveal the information of traps within materials and it could explain the performance of persistence. As shown in Figure 6, TL curves are quite different between samples. TL signals from MAO:Fe³⁺ are very scarce which means there are no suitable traps in this material to store energy. It can explain the poor persistent phenomena for MAO:Fe³⁺. The peak appearing in the normalized plot of MAO:Fe³⁺ above 375 °C is the black-body signal from the sample holder. As for sample ZAO:Fe³⁺, although it has the strong TL signal, it only appears at around 300 °C. According to the theory of TL, there is a clear relationship between the effective temperature range of the persistent luminescence decay curves output and the TL glow curves, the trap depth is too high for the carriers to escape at room temperature [29-31]. Thus it is not a good candidate for the persistent material but it might be suitable for the radiation dosimetry material because it has an ideal single TL peak. On the contrary, TL signals from samples of ZGO:Fe³⁺ and MGO:Fe³⁺ are continuously distributed from the low to high temperature range, which proves that the carriers have the chance to escape even at room temperature. TL signals of MGO:Fe³⁺ are the most intense one among the samples which show that the material could supply enough traps for the carriers, and very helpful for the persistent luminescence. According to the studies on the spinel typed persistent material [18, 32], anti-site defects play a very important roles for the TL and afterglow, thus it is speculated that the possible defects are Zn_{Ga}, Ga_{Zn}, Zn_{Al}, Al_{Zn}, Mg_{Ga}, Ga_{Mg}, Mg_{Al}, Al_{Mg}. The results here prove again that TL is a very useful tool to understand the performance of persistent luminescence. Interestingly, the TL and persistent luminescence intensity are in the order of MGO:Fe³⁺ > ZGO:Fe³⁺ > ZAO:Fe³⁺ > MAO:Fe³⁺ here while the afterglow results for the Cr³⁺-doped spinel structure samples are in the order of ZGO:Cr³⁺ > ZAO:Cr³⁺ > MAO:Cr³⁺ > MGO:Cr³⁺ according to other report [32]. It can be noticed that the order is the same for the remaining samples except for the MGO sample. MGO is the worst matrix for Cr³⁺ ions doping but the best for Fe³⁺ ions. Such anomalies could suggest that traps (nature and depth) are not only determined by the matrix itself, but also by the match or mismatch with the dopants. An important factor to remember is that with the high dopant levels of 5 mol% it is highly probable

that the lattices accommodate dopants, not in isolation, but in more efficient arrangements of pairs or other localised groupings.

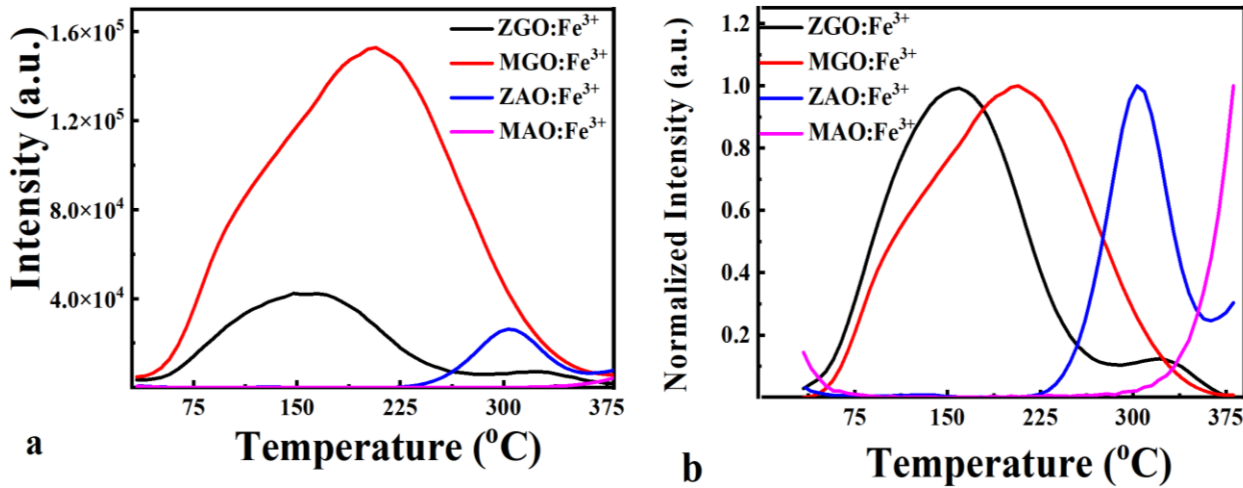


Figure 6a. TL glow curves of the Fe doped spinel samples which have been integrated from 600 to 800 nm. 6b. The normalized TL glow curves for easy comparison.

3.4. XPS and EPR analysis

Although it is hard to identify the exact defects which acts as traps for these samples, anti-site defects (Ga_{Zn} , Zn_{Ga} , Ga_{Mg} , Mg_{Ga} , Al_{Zn} , Zn_{Al}) inside these spinel-type material must play an important role. Besides, the structural environment has an impact on the luminescence properties of Fe^{3+} ions which leads to the shift of peak wavelength. Thus, XPS and EPR experiments have been carried out on the iron doped samples to reveal these although it is far from easy to quantify the exact details.

As shown in Figure 7a, the elemental composition of all the iron doped samples, as well as the valence states of the atoms have been indicated according to the XPS data. It can be observed from the results that there are no other impurity elements introduced during the preparation process except the carbon surface contamination for all the samples. Since the doping concentration is low compared with other elements, the peaks of Fe2p are relatively small for all the samples. The enlarged XPS spectra of all metal ions have been presented. Zn2p and Mg1s XPS peaks are shown in Figure 7b. Al2p and Ga2p are in Figure 7c. Fe 2p XPS spectra are in Figure 7d. As mentioned, under certain conditions the spinel-type structures are mixed and the

A- and B- sites atoms occupy randomly both the tetrahedral and octahedral sites. The XPS spectra for the metal ions have all been fitted into two peaks according to the reference binding energies as shown in Figure 7b-7c. These data can reveal the site occupation information and give ones the general idea on the existence of anti-site defects within materials. For Zn2p, it has been reported that the lower binding energy photo electron peaks of the Zn 2p_{1/2} and Zn 2p_{3/2} peaks belongs to the Zn²⁺ ions occupying tetrahedral position, while the relatively higher ones are due to the Zn²⁺ occupying the octahedral position [33, 34]. Peaks of Mg1s located at high and low binding energies can be assigned to Mg²⁺ ions at octahedral and tetrahedral positions respectively [35-37]. Peaks with higher binding energies in Ga2p_{3/2}, Ga2p_{1/2} as well as Al2p are attributed to Ga³⁺ and Al³⁺ ions located in the octahedron and the peaks with lower binding energies are attributed to the ions in the tetrahedron [38-41].

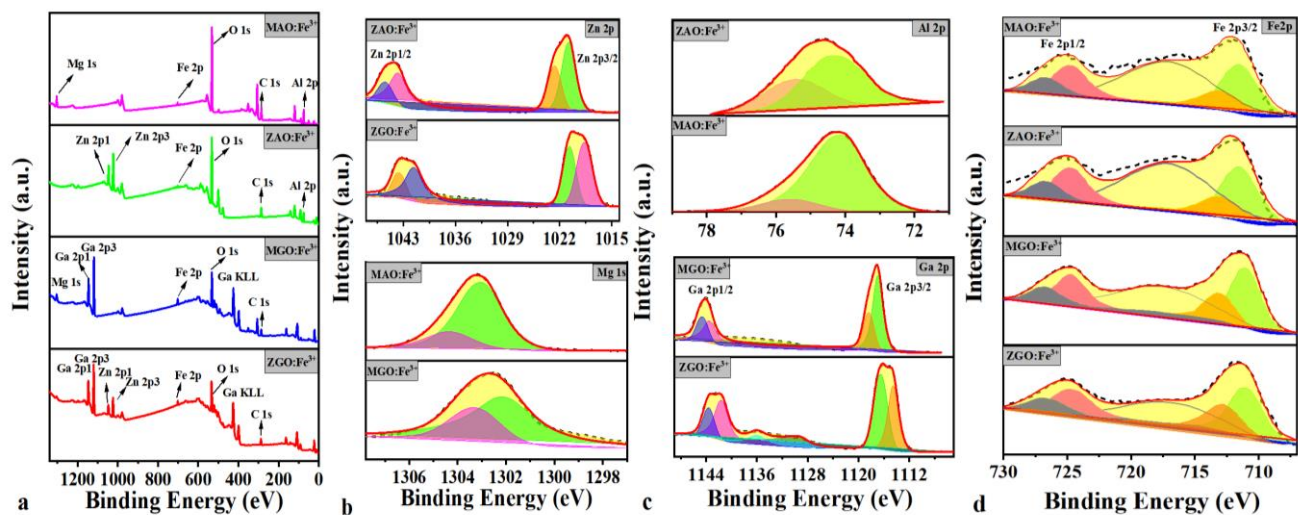


Figure 7a. XPS spectra of four Fe³⁺ doped spinel-type structured luminescent materials. b. Enlarged Zn 2p and Mg 1s XPS spectra. c. Enlarged Ga 2p and Al 2p XPS spectra. d. Enlarged Fe 2p XPS spectra.

As shown in Figure 7d, two main peaks can be identified in both the Fe 2p_{3/2} and Fe 2p_{1/2} peaks. The doped Fe³⁺ ions could occupy both octahedral and tetrahedral sites. Thus, two main peaks are de-convoluted according to the reference data and the percentages have been calculated, as shown in Table I. The calculated peak area percentage of Fe ions occupying tetrahedral positions for ZGO:Fe³⁺, MGO:Fe³⁺, ZAO:Fe³⁺ and MAO:Fe³⁺ samples are 36%, 34%, 36% and 37% respectively which are smaller than the ones of octahedral sites. Thus, for these samples, Fe³⁺ ions are more likely to occupy octahedral lattice

positions.

Table I. XPS data of Fe2p for ZGO:Fe³⁺, MGO:Fe³⁺, ZAO:Fe³⁺ and MAO:Fe³⁺ samples.

Element/ Transition	Binding energy (± 0.1 eV)	Area percent	samples
Fe2p	711.5	Fe(oct)=64.39%	ZnGa ₂ O ₄
	713		
	716.9	satellite peaks ^[41]	
	724	Fe(tet)=35.61%	
	726.7		
Fe 2p	710.6	Fe(oct)=65.7%	MgGa ₂ O ₄
	712.8		
	717.5	satellite peaks	
	724.6	Fe(tet)=34.3%	
	726.5		
Fe 2p	710.7	Fe(oct)=63.90%	ZnAl ₂ O ₄
	712.4		
	716.8	satellite peaks	
	724.4	Fe(tet)=36.10%	
	726.5		
Fe 2p	710.8	Fe(oct)=62.95%	MgAl ₂ O ₄
	712.8		
	717	satellite peaks	
	724.5	Fe(tet)=37.05%	
	726.8		

EPR measurements were carried out to further confirm the occupancy situation of Fe³⁺ ions in spinel-type structured luminescent materials. The obtained results are shown in [Figure 8](#). There are multiple resonance absorption lines collected which confirms that Fe³⁺ ions are in different crystal field environments. Such as for ZGO: Fe³⁺, the resonance signals of Fe³⁺ with the magnetic field around 100 to 150 mT area with high g value (4.45) might be attributed to Fe³⁺ ions in the tetrahedral sites and the lower g value (2.05) are attributed to Fe³⁺ ions in the octahedral sites [\[21, 22\]](#). The similar resonance signals could be attributed to the samples of MGO:Fe³⁺, ZAO:Fe³⁺ and MAO:Fe³⁺ [\[42, 43\]](#). The data offer a simplistic view of the site

structures but once again it must be emphasized that for high dopant levels there are long range interactions which add complexity to the analysis.

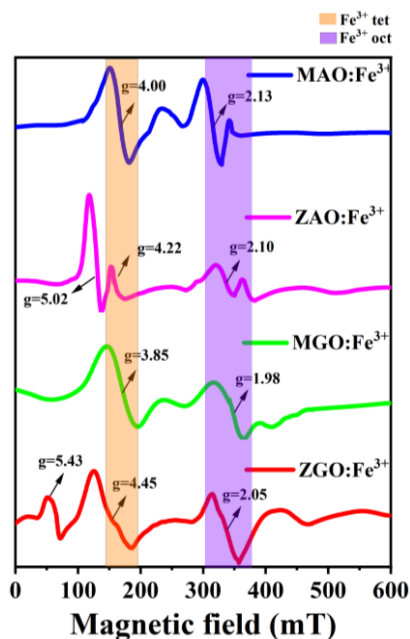


Figure 8. EPR signals of four Fe³⁺ doped spinel-type structured luminescent materials.

4. Conclusion

The Fe doped NIR PersL spinel type-based compounds AB₂O₄ with A = Zn, Mg and B = Ga, Al were successfully obtained through a high temperature solid phase method. The crystal structure, photoluminescence, PersL, and TL of the four samples were studied. PL emission spectra results show infrared emission from 600 to 900 nm for all four samples with spinel structure. The persistent luminescence decay curves show that MGO:Fe³⁺ and ZGO:Fe³⁺ have relative good PersL characteristics. MGO:Fe³⁺ is a very good candidate for applications since its PersL duration time is more than 16 h. It is demonstrated by the XPS and EPR results that Fe³⁺ ions tend to occupy the octahedral positions. This work provides ideas for the study luminescence mechanism of Fe-doped materials and the ways to enhance their luminescence efficiency. Moreover, Fe³⁺ ions are cheap and readily available, non-toxic and harmless. Thus Fe³⁺-doped MGO phosphors can replace the commonly used Cr³⁺-activated NIR PersL materials. Therefore, this work should lead to the development of new PersL materials for bioimaging and agriculture applications.

Reference

- [1] J. Xu, S. Tanabe, Persistent luminescence instead of phosphorescence: History, mechanism, and perspective, *J. Lumin.* 205 (2019) 581-620. <https://doi.org/10.1016/j.jlumin.2018.09.047>.
- [2] J. Xu, D. Murata, J. Ueda, B. Viana, S. Tanabe, Toward Rechargeable Persistent Luminescence for the First and Third Biological Windows via Persistent Energy Transfer and Electron Trap Redistribution, *Inorg. Chem.* 57 (2018) 5194. <https://doi.org/10.1021/acs.inorgchem.8b00218>.
- [3] Y. Jin, Y. Hu, L. Yuan, L. Chen, H. Wu, G. Ju, H. Duan, Z. Mu, Multifunctional near-infrared emitting Cr³⁺-doped Mg₄Ga₈Ge₂O₂₀ particles with long persistent and photostimulated persistent luminescence, and photochromic properties, *J. Mater. Chem. C* 4 (2016) 6614. <https://doi.org/10.1039/C6TC01640E>.
- [4] Y. Li, S. Zhou, Y. Li, K. Sharafudeen, Z. Ma, G. Dong, M. Peng, J. Qiu, Long persistent and photo-stimulated luminescence in Cr³⁺-doped Zn–Ga–Sn–O phosphors for deep and reproducible tissue imaging, *J. Mater. Chem. C* 2 (2014) 2657. <https://doi.org/10.1039/C4TC00014E>.
- [5] D. Poelman, D.V.D. Heggen, J. Du, E. Cosaert, P.F. Smet, Persistent phosphors for the future: Fit for the right application, *J. Appl. Phys.* 128 (2020) 240903. <https://doi.org/10.1063/5.0032972>.
- [6] A. Bessière, S. Jacquart, K. Priolkar, A. Lecointre, B. Viana, D. Gourier, ZnGa₂O₄:Cr³⁺: A new red long-lasting phosphor with high brightness, *Opt. Express*. 19 (2011) 10131-10137. <https://doi.org/10.1364/OE.19.010131>.
- [7] Y. Jiang, Y. Li, C. Richard, D. Scherman, Y. Liu, Hemocompatibility investigation and improvement of near- infrared persistent luminescent nanoparticle ZnGa₂O₄:Cr³⁺ by surface PEGylation, *J. Mater. Chem. B* 7 (2019) 3796-3803. <https://doi.org/10.1039/C9TB00378A>.
- [8] N. W. Johnson, J.A. McLeod, A. Moewes, The electronic structure of lithium metagallate, *J. Phys. Condens. Matter*. 23 (2011) 445501. <https://doi.org/10.1088/0953-8984/23/44/445501>.
- [9] S. S. Lin, H. Lin, Q. M. Huang, Y. Cheng, J. Xu, J. M. Wang, X. Q. Xiang, C. Y. Wang, L. Q. Zhang, Y. S. Wang, A Photostimulated BaSi₂O₅:Eu²⁺,Nd³⁺ Phosphor-in-Glass for Erasable-Rewritable Optical Storage Medium, *Laser Photonics Rev.* 13 (2019) 1900006. <https://doi.org/10.1002/lpor.201900006>.
- [10] C. Wang, Y. Jin, Y. Lv, G. Ju, D. Liu, L. Chen, Z. Li, Y. Hu, Trap distribution tailoring guided design of super-long-persistent phosphor Ba₂SiO₄:Eu²⁺,Ho³⁺ and photostimulable luminescence for optical information storage, *J. Mater. Chem. C* 6 (2018) 6058-6067. <https://doi.org/10.1039/C8TC01722K>.

- [11] Y.J. Li, Y.Y. Ma, S. Ye, G.P. Hu, Q.Y. Zhang, Site-related near-infrared luminescence in MAl_2O_9 ($\text{M} = \text{Ca}, \text{Sr}, \text{Ba}$): Fe^{3+} phosphors, *Mater. Res. Bull.* 51 (2014) 1-5. <https://doi.org/10.1016/j.materresbull.2013.11.008>.
- [12] Y. Zhuang, S. Tanabe, L. Pickney, Conversion of Valence State and Coordination State of Fe in Transparent Glass-Ceramics Containing $\text{Li}_2\text{ZnSiO}_4$ Nanocrystals, *J. Am. Ceram. Soc.* 96 (2013) 2864-2869. <https://doi.org/10.1111/jace.12398>.
- [13] L. P. Sosman, P. S. Silva, T. Abritta, Optical Spectroscopy of $\text{MgGa}_2\text{O}_4:\text{Fe}^{3+}$, *Phys. Stat. Sol.* 176 (1999) 1085-1089. [https://doi.org/10.1002/\(SICI\)1521-396X\(199912\)176:2<1085::AID-PSSA1085>3.0.CO;2-P](https://doi.org/10.1002/(SICI)1521-396X(199912)176:2<1085::AID-PSSA1085>3.0.CO;2-P).
- [14] R. Kang, X.J. Dou, H.W. Lian, Y. Li, $\text{SrAl}_2\text{O}_9:\text{Fe}^{3+}$ @3-aminopropyl triethoxysilane: Ambient aqueous stable near-infrared persistent luminescent nanocomposites, *J. Am. Ceram. Soc.* 103 (2019) 258-265. <https://doi.org/10.1111/jace.16707>.
- [15] Z.H. Zhou, S. Zhang, Y.K. Le, H. Ming, Y. Li, S. Ye, M.Y. Peng, J.R. Qiu, G.P. Dong, Defect Enrichment in Near Inverse Spinel Configuration to Enhance the Persistent Luminescence of Fe^{3+} , *Adv. Optical Mater.* 1 (2021) 2101669. <https://doi.org/10.1002/adom.202101669>.
- [16] Z.H. Zhou, X.D. Yi, P.X. Xiong, X.Y. Xu, Z.J. Ma, M.Y. Peng, Cr^{3+} -free near-infrared persistent luminescence material $\text{LiGaO}_2:\text{Fe}^{3+}$: optical properties, afterglow mechanism and potential bioimaging, *J. Name.* 8 (2020) 14100-14108. <https://doi.org/10.1039/D0TC03212C>.
- [17] B. Jiang, F. Chi, X. Wei, Y. Chen, M. Yin, A self-activated MgGa_2O_4 for persistent luminescence phosphor, *J. Appl. Phys.* 124 (2018) 063101. <https://doi.org/10.1063/1.5024771>.
- [18] A. Bessière, S.K. Sharma, N. Basavaraju, K.R. Priolkar, L. Binet, B. Viana, A.J.J. Bos, T. Maldiney, C. Richard, D. Scherman, D. Gourier, Storage of visible light for long-lasting phosphorescence in chromium-doped zinc gallate, *Chem. Mater.* 26 (2014) 1365. <https://doi.org/10.1021/cm403050q>.
- [19] M. Allix, S. Chenu, E. Véron, F. Porcher, D. Massiot, Considerable improvement of long-persistent luminescence in germanium and tin substituted ZnGa_2O_4 , *Chem. Mater.* 25 (2013) 1600-1606. <https://doi.org/10.1142/S0217984916>.
- [20] Z.H. Zhou, X.D. Yi, P.X. Xiong, X.Y. Xu, Z.J. Ma, M.Y. Peng, Cr^{3+} -Free near-infrared persistent luminescence material $\text{LiGaO}_2:\text{Fe}^{3+}$: optical properties, afterglow mechanism and potential bioimaging, *J. Mater. Chem. C.* 8 (2018) 14100. <https://doi.org/10.1039/d0tc03212c>.
- [21] T.R.N. Kutty, M. Nayak, Cation coordination and Fe^{3+} luminescence in LiAlO_2 polymorphs prepared by a hydrothermal method, *Mater. Res. Bull.* 34 (1999) 249-262. [https://doi.org/10.1016/S0025-5408\(99\)00014-8](https://doi.org/10.1016/S0025-5408(99)00014-8).

- [22] M. Nayak, T.R.N. Kutty, Luminescence of Fe³⁺ doped NaAlSiO₄ prepared by gel to crystallite conversion, *Mater. Chem. Phys.* 57 (1998) 138–146. [https://doi.org/10.1016/S0254-0584\(98\)00209-0](https://doi.org/10.1016/S0254-0584(98)00209-0).
- [23] G.T. Pott, B.D. Menicol, The luminescence of Fe³⁺ and Cr³⁺ IN α -gallia, *J. Lumin.* 6 (1973) 225–228. [https://doi.org/10.1016/0022-2313\(73\)90122-1](https://doi.org/10.1016/0022-2313(73)90122-1).
- [24] L. P. Sosman , A. Dias Tavares, Jr, P. S. Silva , T. Abritta, Optical Spectroscopy of MgGa₂O₄ : Fe³⁺, *phys. stat. sol. (a)* 176 (1999) 1085. 10.1002/(SICI)1521-396X(199912)176:23.0.CO;2-P.
- [25] Z. Long, Y. Wen, J. Zhou, J. Qiu, H. Wu, X. Xu, X. Yu, D. Zhou, J. Yu, Q. Wang, No-interference reading for optical information storage and ultra-multiple anti-counterfeiting applications by designing targeted recombination in charge carrier trapping phosphors, *Adv. Opt. Mater.* 7 (2019) 1900006. <https://doi.org/10.1002/adom.201900006>.
- [26] Y.J. Liang, F.Liu, Y.F. Chen, X.J. Wang, K.N. Sun, Z. Pan, New function of the Yb³⁺ ion as an efficient emitter of persistent luminescence in the short-wave infrared, *Light Sci Appl.* 5 (2016) e16124. <https://doi.org/10.1038/Isa.2016.124>.
- [27] F. Liu, Y. Liang, Y. Chen, Z. Pan, Divalent Nickel-Activated Gallate-Based Persistent Phosphors in the Short-Wave Infrared, *Adv. Opt. Mater.* 4 (2016) 562-566. <https://doi.org/10.1002/adom.201500656>.
- [28] L. Xu, Y. Su, Q.T. Zhou, S. Li, Y.Q. Chen, Y.i Feng, Self-Assembled Catalyst Growth and Optical Properties of Single-Crystalline ZnGa₂O₄ Nanowires Cryst, *Growth Des.* 7 (2007) 810. <http://doi.org/10.1021/cg0603568>.
- [29] J. Du, O.Q. Clercq, D. Poelman, Temperature dependent persistent luminescence: Evaluating the optimum working temperature. *Sci. Rep.* 9 (2019) 10517. <https://doi.org/10.1038/s41598-019-46889-z>.
- [30] C.L. Wang, Y.H. Jin, J.X. Zhang, X.G. Li, H.Y. Wu, R.T. Zhang, Q. Yao, Y.H. Hu, Linear charging-discharging of an ultralong UVA persistent phosphor for advanced optical data storage and wide-wavelength-range detector. *Chem. Eng. J.* 453 (2023) 139558. <https://doi.org/10.1016/j.cej.2022.139558>.
- [31] Songlu Tian, Peng Feng, Songsong Ding, Yajie Wang, Yuhua Wang, A color-tunable persistent luminescence material LiTaO₃:Pr³⁺ for dynamic anti-counterfeiting. *J. Alloy. Compd.* 902 (2022) 163776. <https://doi.org/10.1016/j.jallcom.2021.163325>.
- [32] S.K. Sharma, D. Gourier, B. Viana, T Maldiney, E Teston, D Scherman, Persistent luminescence of AB₂O₄: Cr³⁺ (A= Zn, Mg, B= Ga, Al) spinels: new biomarkers for in vivo imaging. *Opt. Mater.* 2014, 36(11): 1901-1906.
- [33] D. Zhang, Q. Guo, Y. Ren, C. Wang, Q. Shi, Q. Wang, X. Xiao, W. Wang, Q. Fan, Influence of inversion defects and Cr–Cr pairs on the photoluminescent performance of ZnAl₂O₄ crystals, *J. Sol–Gel Sci. Technol.* 85 (2018) 121–131.

<http://doi.org/10.1007/s10971-017-4527-4>.

- [34] D. Zhang, C. Du, J. Chen, Q. Shi, Q. Wang, S. Li, W. Wang, X. Yan, Q. Fan, Improvement of structural and optical properties of $\text{ZnAl}_2\text{O}_4:\text{Cr}^{3+}$ ceramics with surface modification by using various concentrations of zinc acetate, *J. Sol–Gel Sci. Technol.* 88 (2018) 422–429. <http://doi.org/10.1016/j.matdes.2016.11.034>.
- [35] P.A. Kumar, M.P. Reddy, B.H. Bae Hyun-Sook, H.H. Phil, Influence of Mg Addition on the Catalytic Activity of Alumina Supported Ag for C_3H_6 -SCR of NO, *Catal. Lett.* 131 (2009) 85–97. <https://doi.org/10.1007/s10562-009-9895-0>.
- [36] R. Brambilla, C. Radtke, J.H.Z. Dos Santos, M.S.L. Miranda, An investigation on structure and texture of silica-magnesia xerogels, *J. Sol–Gel Sci. Technol.* 51 (2009) 70–77. <https://doi.org/10.1007/s10971-009-1937-y>.
- [37] X.L. Duan, J. Liu, F.P. Yu, X.Q. Wang, Co/Cr co-doped MgGa_2O_4 nanoparticles: Microstructure and optical properties, *Mater. Res. Bull.* 73 (2016) 90–95. <https://doi.org/10.1016/j.materresbull.2015.08.031>.
- [38] Z. Gong, Y. Liu Y, J. Yang, D. Yan, H.C. Zhu, C.G. Liu, C.S. Xu, H. Zhang. A Pr^{3+} doping strategy for simultaneously optimizing the size and near infrared persistent luminescence of $\text{ZGGO}:\text{Cr}^{3+}$ nanoparticles for potential bio-imaging, *Phys. Chem. Chem. Physics.* 19 (2017) 24513. <http://doi.org/10.1039/C7CP02909H>
- [39] K.G. Tshabalala, S.H. Cho, J.K. Park, S.S. Pitale, I.M. Nagpure, R.E. Kroon, H.C. Swart, O.M. Ntwaeaborwa, Luminescent properties and X-ray photoelectron spectroscopy study of $\text{ZnAl}_2\text{O}_4:\text{Ce}^{3+}, \text{Tb}^{3+}$ phosphor, *J Alloys Comp* 509 (2011) 10115–10120. <https://doi.org/10.1016/j.mallcom.2011.8.054>.
- [40] B. Chornik, M. Seguel, L. Flores, lillo, C. Caro, Sandoval, A photochemical proposal for the preparation of ZnAl_2O_4 and MgAl_2O_4 thin films from b-diketonate complex precursors, *Mater. Res. Bull.* 77 (2016) 212–220. <https://doi.org/10.1016/j.materresbull.2016.01.044>.
- [41] S.N. Ogugua, O.M. Ntwaeaborwa, H.C. Swart, Luminescence, structure and insight on the inversion degree from normal to inverse spinel in a $\text{ZnAl}_{(2-x)}\text{Fe}_x^{3+}\text{O}_4$ system, *Bol. Soc. Esp. Ceram.* V. 147 (2021) 0366. <https://doi.org/10.1016/j.bsecv.2020.02.005>.
- [42] I. Ardelean, P. Pascuta, L.V. Giurgiu, EPR and Magnetic Susceptibility Investigations of $\text{Fe}_2\text{O}_3\text{-B}_2\text{O}_3\text{-KCl}$ Glasses, *Int J. Mod. Phys B.* 17 (2003) 3049. <https://doi.org/10.1142/S0217979203020648>.
- [43] E. Burzo, I. Ardelean, I. Ursu, On the physical properties of $20\text{Fe}_2\text{C380} [3\text{B}_2\text{O}_3 (1-x)\text{PbO } x \text{GeO}_2]$, *J. Mater. Sci.* 15 (1980) 581. <https://doi.org/10.1007/BF00551720>.